ChemElectroChem

Review
doi.org/10.1002/celc.202400482

Chemistry Europe
European Chemical Societies Publishing

www.chemelectrochem.org

Design Strategies to Enhance Copper Electrocatalytic Performance for Nitrate-to-Ammonia Electroreduction

Simone Lombardi,[a] Silvia Mostoni,[a] Lorenzo Mirizzi,[a] Roberto Scotti,[a] Rosanna Viscardi,[b] Mohsin Muhyuddin,[a] Massimiliano D'Arienzo,*[a] and Carlo Santoro*[a]

Electrochemical nitrate reduction (NO_3^-RR) is being recognized as a sustainable approach to synthesizing ammonia which is essential for the chemical industry and a key agricultural input conventionally produced through the hard-to-abate Haber Bosch process. Among various transition metals, copper-based electrocatalysts stand out in efficaciously carrying out this reaction owing to their superior electrocatalytic activity and selectivity. In this context, here, current state of research and advanced scientific understandings of employing Copper for NO_3^-RR are succinctly, but comprehensively, presented while focusing on its design strategies to enhance the electrocatalytic performance. First, the NO_3^-RR reaction mechanisms taking place at the surface of copper are described, followed by a discussion of its unique attributes in facilitating ammonia electrosynthesis. Then, various electrocatalyst fabrication routes and designing strategies are reviewed, emphasizing the role of the evolved structure, morphology, textural properties and surface chemistries in improving the reaction kinetics. Nanostructuring, facet and defect engineering, support, doping, alloying, heterojunction and the role of single active catalysts (SACs) centers as the key parameters for enhanced electrocatalytic behavior are highlighted.

1. Introduction

Ammonia (NH_3) is widely used as fertilizer, energy carrier, and reagent in various chemical syntheses[1] Ammonia is the building block for urea which is the most used nitrogen-based fertilizer worldwide.[2] Recently, NH_3 has also gained attention as a promising next-generation carbon-free energy carrier, thanks to its high energy density (11.2 MJ L^{-1}), which is comparable to that of nonrenewable energy sources.[3] Moreover, as a hydrogen derivative, it holds significant potential to address and simplify future challenges related to the storage and transportation of H_2 energy; in fact, its high volumetric hydrogen density, low storage pressure and stability for long-term storage are among the beneficial characteristics of ammonia for hydrogen storage.[4] The annual global production is estimated to be 150 million tons, and it is expected to increase,[5] making it the world's second most commonly produced chemical after sulfuric acid (H_2SO_4). NH_3 production is commonly based on the Haber Bosch process, an energy-intensive process (>600 KJ mol^{-1} ammonia), which entails demanding conditions of high pressures and high temperatures (150-350 atm, 350–550 °C).[6] Additionally, in this process, H_2 is entirely produced through steam reforming of natural gas, which consumes 3–5% of the global natural gas supply and is responsible for 450 million metric tons of CO_2 emission annually.[7]

Consequently, researchers have started exploring low-carbon and environmentally friendly methods for NH_3 production that can operate under ambient temperature and pressure. Among the various strategies to produce ammonia, the nitrogen reduction reaction (NRR) can be an effective approach, using nitrogen, abundant in the atmosphere, as a reagent, renewable electricity as the energy source under mild conditions, and water as the hydrogen source.[8] However, the high bond energy (941 kJ mol^{-1}) of the N≡N bond, the low solubility of N_2 in water, and the competitive hydrogen evolution reaction (HER) seriously hinder the development and application of this technology to produce ammonia from nitrogen gas.[9]

In addition to the challenges associated with conventional NH_3 production, nitrate pollution of surface and groundwater is becoming an increasing issue, due to the potential damage to the ecosystem, causing eutrophication and human health issues.[10] In fact, a by-product of its incomplete conversion, nitrite (NO_2—), is considered carcinogenic due to its associations with gastrointestinal cancers, particularly gastric and esophageal cancer. This elevated risk is attributed to the formation of carcinogenic nitrosamines within the body.[11] Additionally, it can cause methemoglobinemia, a condition that severely reduces the blood's ability to transport oxygen, leading to symptoms such as symptoms like cyanosis and respiratory distress.[12]

For these reasons, the United States Environmental Protection Agency (US EPA) and the World Health Organization (WHO) recommend that the concentration of nitrate (NO_3^-) in drinking water should not exceed 10.0 mg of nitrogen per liter (mg N L^{-1}).[13]

[a] S. Lombardi, S. Mostoni, L. Mirizzi, R. Scotti, M. Muhyuddin, Prof. M. D'Arienzo, Prof. C. Santoro
Department of Materials Science, University of Milano-Bicocca U5, Via Roberto Cozzi 55, 20125, Milano (Italy)
E-mail: massimiliano.darienzo@unimib.it
carlo.santoro@unimib.it

[b] R. Viscardi
Casaccia Research Center, ENEA, Department of Energy Technologies and Renewable Sources, Via Anguillarese 301, 00123 Santa Maria di Galeria, 00123, Rome, Italy

Although some conventional technologies such as ion exchange, biological denitrification and electrodialysis have been applied for nitrate removal,[14] technical limitations including low efficiency and high post-treatment costs limit their practical applications.

Recently, the electrochemical reduction of nitrate to ammonia (NO_3^-RR) has received extensive attention due to its ability to simultaneously synthesize NH_3 under ambient conditions and remove nitrates from the environment. Unlike N_2, the high solubility of NO_3^- in water and the low bond energy of

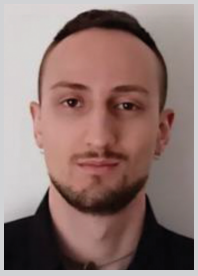

Simone Lombardi is a PhD student in Materials Science and Nanotechnology at the University of Milano-Bicocca jointly with ENEA. His research focuses on the electrochemical production of hydrogen and small molecules using platinum group metal-free electrocatalysts. In 2022, he earned the Bachelor of Science degree in Chemical Sciences and Technologies. In 2024, he obtained a Master of Science degree cum laude in Chemical Sciences and Technologies, after conducting research on mixed zinc and copper oxides for electrochemical nitrate reduction to ammonia.

Silvia Mostoni earned a MSc degree in Chemistry at the University of Milano in 2015 working on inorganic nanoparticles with photocatalytic properties. She then moved to the University of Milano Bicocca, where she received her PhD in 2019, developing inorganic zinc-based activators for rubber curing. Since 2023 she is a Researcher at the University of Milano Bicocca. Her research interests focus on the synthesis, characterization and surface functionalization of metal oxide nanoparticles for application for catalysis and photocatalysis, automotive and energetic sector and luminescent materials. She has 39 manuscripts ($H_{index}=11$) and holds 2 patents.

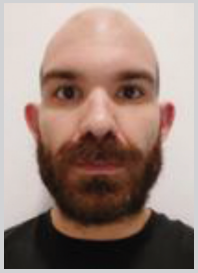

Lorenzo Mirizzi hold a PhD in Material Science and Nanotechnology focusing on inorganic materials for heat management in elastomeric composites. He received a Bachelor of Science degree in chemistry at the University of Bari and a Master of Science degree in Photochemistry and Molecular Materials at the University of Bologna. He worked as a postdoctoral researcher on the synthesis of electrocatalysts for electrolyzer, fuel cell and reduction of nitrate to ammonia. He is currently a member of the research and development team at Directa Plus Spa. He is interested in new applications of graphene.

Roberto Scotti received his master's degree in industrial chemistry at the University of Milano. He worked at the company EniRicerche and since 2005 is Associate Professor of General and Inorganic Chemistry at University of Milano-Bicocca, where since 2021 he has been Dean of the Course of Chemistry Science and Technology. The main research interests are focused on the design and synthesis of inorganic and hybrid materials, with controlled structure, morphology, surface characteristics and defectivity for application in catalysis, photocatalysis, composites for automotive, metal recovering. He is author of 150 publications (Hindex = 39), 13 patents and 10 book chapters.

Rosanna Viscardi completed in 2009 her PhD thesis in electrochemistry at University of Salerno with a work developed in collaboration with ACTA S.p.A about the production of hydrogen by small-molecules electrolysis as water and ammonia. She worked in the renewable energy industry for 6 years where she developed industrial processes for the production of electrocatalysts for alkaline fuel cells and electrolyzers. Since 2012 she is a Researcher of ENEA at Casaccia Research Center. Her research is concentrated in the field of renewable energy, in particular in fuel cells, hydrogen production and the development and understanding of new processes and technologies for the capture and conversion of carbon dioxide into fuels and chemicals.

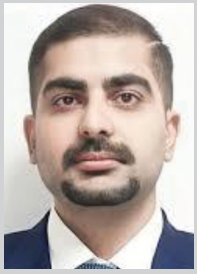

Mohsin Muhyuddin is a committed young researcher specializing in platinum group metal-free (PGM-free) electrocatalysts for green energy and sustainable fuels. He earned his Bachelor's and Master's degrees in Materials Science and Engineering from the Institute of Space Technology, Pakistan, in 2016 and 2019, respectively. In 2024, he completed his Ph.D. at the University of Milano-Bicocca (Unimib), Italy, focusing on advanced single-atom and nanostructured electrocatalysts for fuel cells and water electrolyzers. He also endeavored to upcycle the organic waste (biomass and plastics) into efficacious PGM-free electrocatalysts. Presently, he is a Postdoctoral Researcher in the group of Prof. Carlo Santoro (EBLab), contributing to novel studies for sustainable energy technologies.

Massimiliano D'Arienzo is Associate Professor of General and Inorganic Chemistry since 2018 at the Department of Materials Science in the University of Milano-Bicocca. He is a member of NanoMat@Lab group, whose expertise spans from the synthesis by soft chemistry methods of ceramics and inorganic materials with controlled morphological and surface features, to their exploiting in hybrid materials employed in a wide range of applications (e.g. photocatalysis, catalysis, electrocatalysis, LIBs, and automotive). He has published 95 manuscripts (Hindex = 31), 3 book chapters and holds 4 patents.

Carlo Santoro obtained his PhD at the University of Connecticut in 2009, working on microbial fuel cells. He moved to the University of New Mexico in 2013 working on platinum-free electrocatalysts for oxygen reduction reaction and supercapacitive bioelectrochemical systems. Following a spell as a Lecturer at the University of Manchester (2020), he joined the University of Milano-Bicocca in 2021 as an Assistant Professor, where he established the Electrocatalysis and Bioelectrocatalysis Lab (EBLab) that currently counts 1 Post Doc and 8 PhD students. He is currently an Associate Professor and his work focuses on the development of electrocatalysts based on platinum-group metal-free materials for electrochemical systems, pursuing biomimetic and bioinspired approaches. He has published over 140 manuscripts (Hindex = 48) and holds 2 patents.

the N=O bond (204 kJ mol^{-1}) compared to the 941 kJ mol^{-1} of the N≡N bond, make this process more efficient compared to NRR.[15] Besides, if electricity is provided through renewable energy, this process can be considered totally green and could contribute to electrifying, at least partially, an industrial sector such as NH_3 production, which is crucial to reaching the complete decarbonization set by the EU in 2050.[16] (Figure 1).

In this field, the investigation of suitable electrocatalytic materials to boost the efficiency of NO_3^-RR plays a pivotal role in enhancing the reaction kinetics and selectivity. Therefore, a wide range of metal electrocatalysts, including platinum group metals (PGMs), precious metals and first raw transition metals such as Ru,[17] Ir,[18] Pd,[19] Co,[20] Au[21] and so on have recently been explored. Among these, Cu emerged as a promising electrocatalyst to pursue this reaction. In fact, from a reaction dynamics perspective, compared with other metals, it shows a stronger electrocatalytic capability for NO_3^-RR.[22] Furthermore, from an economic point of view, its higher availability and low cost compared to most of the noble metals make it particularly suitable for large-scale application.

In this context, this review aims to summarize the current state of research on copper as an electrocatalyst for the NO_3^-RR, with the ambitious goal of providing some hints on the main design strategies to enhance its performance. In the first part, the NO_3^-RR reaction mechanisms taking place specifically at the surface of copper are described, while other reviews often address the NO_3^-RR mechanism in a more general context.

Additionally, this review includes a discussion of its unique attributes in facilitating ammonia electrosynthesis, an aspect frequently overlooked in less specialized reviews focused on this metal.

Subsequentially, various key parameters that influence its performance are discussed, with a special focus on the role of the structural, morphological and surface properties of the electrocatalysts on their performance.

2. Nitrate Reduction Reaction (NO_3^-RR) Mechanism ON Copper Electrocatalyst

A clear understanding of the electrocatalytic mechanism of NO_3^-RR is essential for designing electrocatalysts with superior activity and selectivity.

The process begins with the migration of nitrate ions (NO_3^-) in the electrolyte toward the electrode surface, where they are adsorbed onto the electrocatalyst, forming adsorbed nitrate ($*NO_3^-$). At the liquid-solid interface, $*NO_3^-$ reacts with water molecules and electrons supplied by the external circuit, undergoing a series of intermediate steps that ultimately convert it into adsorbed ammonia ($*NH_3$). Finally, $*NH_3$ desorbs from the surface of the electrocatalyst, completing the electrochemical conversion of NO_3^- into NH_3.

However, there is inherent competition between the NO_3^-RR and HER. As the overpotential increases, HER dominates, reducing the Faradic efficiency (FE) of ammonia production. During HER, H^+ is consumed through a series of reactions, beginning with the Volmer step, where H^+ is reduced to form *H (eq. 1a). This is followed by either the Heyrovsky step, where *H reacts with H^+ to form H_2 (eq. 1b), or the Tafel step, where two *H species recombine to produce H_2 (eq. 1c).[23]

$$H^+ + e^- \rightarrow {}^*H \text{ (Volmer step)} \quad (1a)$$

$${}^*H + H^+ + e^- \rightarrow H_2 \text{ (Heyrovsky step)} \quad (1b)$$

$$\textit{or } {}^*H + {}^*H \rightarrow H_2 \text{ (Tafel step)} \quad (1c)$$

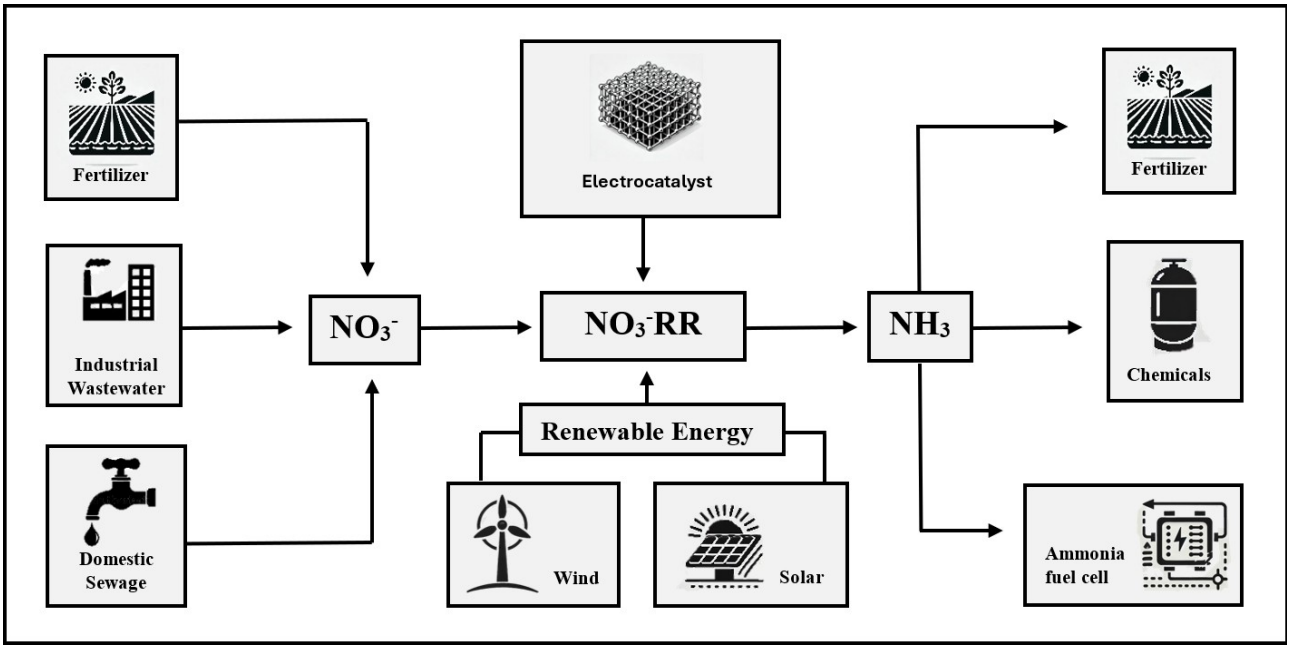

Figure 1. Schematic illustration of sustainable ammonia synthesis via NO_3^-RR

Thus, developing efficient electrocatalysts with specific structures capable of suppressing this competitive reaction is crucial.

The conversion of NO_3^- to NH_3 involves the transfer of eight electrons and multiple reaction intermediates, as nitrogen exhibits a wide range of stable hydrides and oxides with valence states ranging from −3 to +5. The overall reaction can be summarized as follows:[24]

$$NO_3^- + 9H^+ + 8e^- \rightarrow 3H_2O + NH_3 E_0 = 0.88\,V \text{ vs. RHE} \quad (2)$$

Where the potential of 0.88 V *vs* reversible hydrogen electrode (RHE), represents the thermodynamic driving force under standard conditions, indicating the energy required to reduce NO_3^- to NH_3.

Focusing on copper-catalyzed reactions, the mechanism of NO_3^-RR on the surface of copper-based materials can follow two pathways depending upon the different mediation of the reaction, namely, the absorbed atomic hydrogen reduction pathway and electron reduction pathway (Figure 2).

As anticipated, in both pathways, the first step is the adsorption of NO_3^- on the Cu-catalyst surface to obtain adsorbed $*NO_3^-$ species according to *eq. 3:*

$$NO_3^- + * \rightarrow * NO_3^- \quad (3)$$

This first adsorption process is influenced by the mass transfer rate of NO_3^- from the electrolyte to the electrode surface and can also be interfered with by competing anions, such as I^- and Br^-, that decrease the active surface area of the electrode.[25] In the absorbed atomic hydrogen reduction pathway, the atomic hydrogen absorbed on the catalyst surface (H*), which is formed through the reduction of H^+ in the Volmer step *(Eq. 1a)*,[23] deoxygenates $*NO_3^-$ to *N and then hydrogenates *N to $*NH_3$. The main intermediates that are supposed to be involved in these dehydrogenation and hydrogenation reactions are shown in *Eq. 4.1-4.6*. In the last step, $*NH_3$ desorbs from the surface of the electrocatalyst to obtain NH_3. In this pathway, the reaction between $*NO_3^-$ and *H to form $*NO_2^-$ (*Eq. 4.1*) is considered the rate-determining step (RDS).[26]

$$*NO_3^- + 2\,*H \rightarrow * NO_2^- + H_2O \quad (4.1)$$

$$*NO_2^- + 2\,*H \rightarrow * NO + H_2O \quad (4.2)$$

$$*NO + 2\,*H \rightarrow * N + H_2O \quad (4.3)$$

$$*N + *H \rightarrow * NH \quad (4.4)$$

$$*NH + *H \rightarrow * NH_2 \quad (4.5)$$

$$*NH_2 + *H \rightarrow * NH_3 \quad (4.6)$$

In this pathway, it is worth mentioning that parallel reactions may occur, that involve two adjacent *N and $*NH_2$ (produced through *Eq. 4.3* and *Eq. 4.5*, respectively) to form coupled N_2 products, i.e. N_2 and N_2H_4 *(Eq. 5.1–5.2)*. Besides, N_2O may be generated by the combination of *N and *NO (*Eq. 5.3*). Overall, these side reactions contribute to a decrease in the efficiency of ammonia production starting from NO_3^- species. However, Gao et al. reported that, the formation of N–H bonds is kinetically more favorable than the formation of N–N bonds.[27]

Notably, as *H plays a central role in the entire process, this route is favored by electrocatalysts with a high affinity for *H adsorption.

$$*N + *N \rightarrow N_2 \quad (5.1)$$

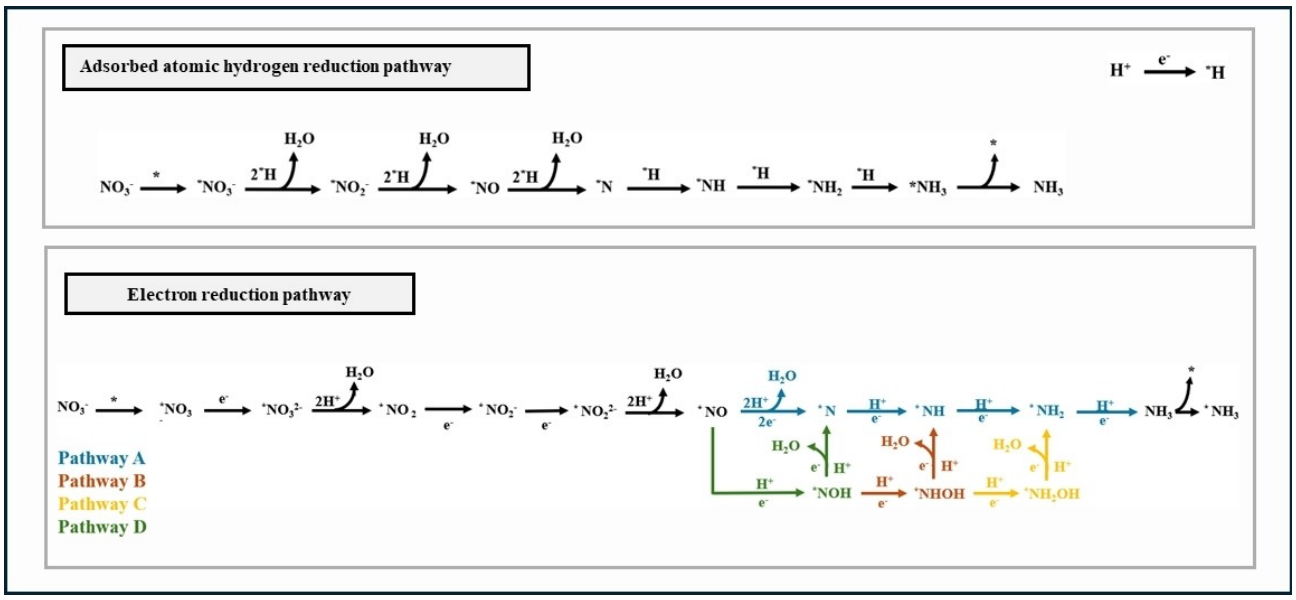

Figure 2. Schematic illustration of the adsorbed atomic hydrogen reduction pathway and electron reduction pathway on copper electrocatalysts

$$^{*}NH_2 + {}^{*}NH_2 \rightarrow N_2H_4 \quad (5.2)$$

$$^{*}N + {}^{*}NO \rightarrow N_2O \quad (5.3)$$

On the other hand, the electron reduction pathway is mediated by electrons. In this route $^{*}NO_3^-$ is initially reduced to $^{*}NO_2^-$ through a three-step mechanism. The process begins with an electron transfer that generates $^{*}NO_3^{2-}$, a short-lived dianion radical (~20 μs), that is immediately hydrolyzed to $^{*}NO_2$. Subsequently, NO_2 undergoes a second electron transfer, resulting in the formation of $^{*}NO_2^-$,[28] a relatively stable intermediate. From this latter intermediate, *NO is formed through an electron transfer to give the unstable anion radical $^{*}NO_2^{2-}$, which rapidly hydrolyzes into *NO.[29]

NO is a crucial intermediate because, from this point, the electron reduction pathway proceeds through a sequence of deoxygenation and hydrogenation reactions. Hu et al.[30] proposed three distinct pathways (Pathways A–C), derived from Density Function Theory (DFT) calculations performed on Cu (111), which is the most stable and commonly exposed surface of copper.

Pathway A is the only pathway that involves the formation of the intermediate N* through the deoxygenation of *NO, followed by step-by-step hydrogenation to $^{*}NH_3$ *(Eq. 6.1–6.3).*

Pathway A:

$$^{*}NO + 2H^+ + 2e^- \rightarrow N + H_2O$$

$$^{*}N + H^+ + e^- \rightarrow {}^{*}NH \quad (6.1)$$

$$^{*}NH + H^+ + e^- \rightarrow {}^{*}NH_2 \quad (6.2)$$

$$^{*}NH_2 + H^+ + e^- \rightarrow {}^{*}NH_3 \quad (6.3)$$

Instead, Pathway B involves the formation of the intermediate *NOH, through the hydrogenation of *NO *(Eq. 7.1)*, followed by a second hydrogenation step, leading to *NHOH *(Eq. 7.2)*. Subsequently, *NHOH undergoes further deoxygenation, producing *NH, *(Eq. 7.3)* which is then hydrogenated step-by-step to form $^{*}NH_2$ and finally $^{*}NH_3$ *(Eq. 7.4 - 7.5)*.

Pathway B:

$$^{*}NO + H^+ + e^- \rightarrow {}^{*}NOH \quad (7.1)$$

$$^{*}NOH + H^+ + e^- \rightarrow {}^{*}NHOH \quad (7.2)$$

$$^{*}NHOH + H^+ + e^- \rightarrow {}^{*}NH + H_2O \quad (7.3)$$

$$^{*}NH + H^+ + e^- \rightarrow {}^{*}NH_2 \quad (7.4)$$

$$^{*}NH_2 + H^+ + e^- \rightarrow {}^{*}NH_3 \quad (7.5)$$

Pathway C is very similar to Pathway B, as it also involves the formation of the intermediates *NOH and *NHOH (*Eq. 7.1–7.2*). However, unlike Pathway B, where *NHOH undergoes deoxygenation to form *NH, in Pathway C, *NHOH is further hydrogenated to produce $^{*}NH_2OH$ *(Eq. 8.1)*. This is then deoxygenated, forming $^{*}NH_2$ and finally hydrogenated to generate $^{*}NH_3$ *(Eq. 8.2-8.3)*.

Pathway C:

$$^{*}NHOH + H^+ + e^- \rightarrow {}^{*}NH_2OH \quad (8.1)$$

$$^{*}NH_2OH + H^+ + e^- \rightarrow {}^{*}NH_2 + H_2O \quad (8.2)$$

$$^{*}NH_2 + H^+ + e^- \rightarrow {}^{*}NH_3 \quad (8.3)$$

Notably, $^{*}NH_2OH$ easily desorbs from the catalyst surfaces, and its detection as a byproduct provided evidence for the existence of this pathway.[31]

In terms of thermodynamics, under the defined condition of pH = 0, Pathway A appears more favorable compared to Pathways B and C. However, the transition from *NO to *N in Pathway A requires a high activation energy of 1.62 eV, making it kinetically sluggish. This energy barrier is significantly larger than the activation energy of 0,08 eV for the transition from *NO to *NOH in Pathways B and C. These differences in activation energies suggest that, although Pathway A is thermodynamically favorable, the kinetic limitations render it less efficient. Moreover, Pathway B involves a hydrogenation step converting *NHOH to $^{*}NH_2OH$ with a high activation energy of 1.36 eV, much greater than the 0.23 eV required for the deoxygenation of *NHOH to *NH in Pathway C.

Considering both thermodynamics and kinetics, pathway C emerges as the most favorable pathway on Cu (111) at pH = 0. Recently, Karamad et. al[22] proposed an alternative pathway (pathway D), always derived from DFT calculations and performed on the Cu (111) surface. In this pathway, the reduction of *NOH formed via the hydrogenation of *NO (*Eq. 7.1*), leads to the formation of *N instead of *NHOH, followed by step-by-step hydrogenation to $^{*}NH_3$. *(Eq. 9.1-9.4)*

Pathway D:

$$^{*}NOH + H^+ + e^- \rightarrow {}^{*}N + H_2O \quad (9.1)$$

$$^{*}N + H^+ + e^- \rightarrow {}^{*}NH \quad (9.2)$$

$$^{*}NH + H^+ + e^- \rightarrow {}^{*}NH_2 \quad (9.3)$$

$$^{*}NH_2 + H^+ + e^- \rightarrow {}^{*}NH_3 \quad (9.4)$$

Koper et al.[32] conducted a comparative study to determine the reactivity of NO_3^- on different transition metals (TMs) and observed that the Tafel slope for most of them, including Cu, was slightly higher than 120 mV/dec.

Based on this observation and supported by the kinetic order and the effect of co-adsorbing anions, the authors proposed that the reduction of $^{*}NO_3^-$ to $^{*}NO_2^-$ is the RDS of the electron reduction pathway. The slow kinetics of this step are attributed to the high energy of the lowest unoccupied molecular π* orbital (LUMO π*) of $^{*}NO_3^-$, in which electrons are difficult to transfer from the electrode surface. However, since Cu presents highly occupied d orbitals, whose energy is similar

to the LUMO π* of *NO_3^-, it facilitates electron transfer and promotes faster kinetics.[33]

Whether the electrocatalyst favors the absorbed atomic hydrogen reduction pathway or the electron reduction pathway depends on the specific characteristics of the catalyst.

For example, for composite catalysts obtained by combining Cu with metals that exhibit a high affinity for adsorbing *H, such as Rh,[34] the reaction is more likely to proceed via the absorbed atomic hydrogen reduction pathway. In contrast, due to the undesirable adsorption of H* on the surface of Cu,[35] the electron transfer pathway is considered the most effective.

However, current mechanistic studies on NO_3^-RR over Cu are limited, with much of the understanding extrapolated from studies on Pt-based catalysts. Thus, further research is needed to elucidate the electrocatalytic mechanism of NO_3^- reduction to NH_3 specifically on Cu.

3. Selection of the Optimum Metal

Copper has been widely investigated as a potential electrocatalytic material for this reaction, both computationally and experimentally. However, besides the fast kinetics of Cu in the RDS of the reduction of *NO_3^- to *NO_2^-, less attention has been paid to understanding the reasons behind such activity and selectivity.

For this reason, Karamad et al.[22] used DFT calculations to identify the TMs among Au, Ag, Cu, Pt, Pd, Ni, Ir, Rh, Ru, and Co, exhibiting higher activity and selectivity towards NO_3^-RR.

NO_3^-RR involves two sets of adsorbates: those that interact with the electrocatalyst surface via the N atom and those that interact via the O atom. *NO and *OH were used as descriptors for the first and second sets, respectively, because the calculated adsorption energies for *N and *O intermediates on TMs scale linearly with those of *NO and *OH, respectively.[36,37]

Using the scaling relation between the adsorbates derived for both sets, rationalized through the d-band model and the position of the d-band center,[38] a Volcano-type relationship between the limiting potential (U_L) and the adsorption energies of *NO and *OH was then constructed (Figure 3a, b). U_L represents here the lowest potential, at which all the reaction steps are downhill in free energy and each line in the graph corresponds to an elementary reaction.

The Potential Limiting Step (PLS) for NO_3^-RR corresponds to the elementary reaction with the most negative U_L and the difference between that and the equilibrium potential defines the overpotential required to drive the NO_3RR.

The Volcano plot in Figure 3a shows that Cu is close to the cusp of the *NO→*NOH line, suggesting a higher electrocatalytic activity compared to the other transition metals considered.

Cu still has an overpotential of 1.11 V and higher activities could be achieved by finding a material that has a weaker *NO binding energy. However, weaker *NO binding energies could lead to the desorption of *NO, thus inhibiting the formation of NH_3, furthermore, the slope of the *NO→*NOH line indicates that the activity is barely affected by changing the *NO binding energy.

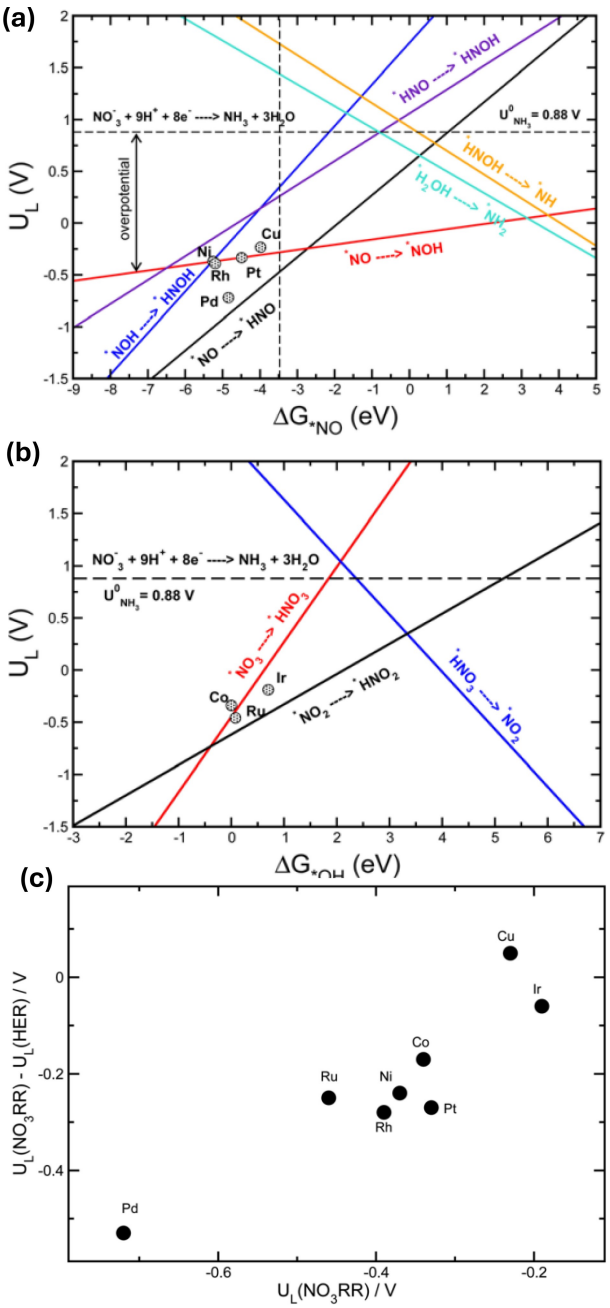

Figure 3. Volcano plot showing limiting potentials for (a) Ni, Rh, Pt, Pd and Cu based on binding energies of NO and (b) Co, Ru and Ir based on binding energies of OH. The horizontal dashed lines in (a) and (b) depict the equilibrium potential for the NO_3^-RR to ammonia. The vertical dashed line in (a) depicts the Gibbs free energy of NO. (c) The difference between the limiting potential for the NO_3^-RR and HER, U_L (NO_3RR) − U_L(HER), is plotted against the limiting potential for the NO_3^-RR, U_L(NO_3RR), for different transition metals (reproduced from,[22] Copyright 2023, Royal Society of Chemistry, licenced under CC BY-NC 3.0).

The Volcano plot in Figure 3b shows that Ir is close to the cusp of *NO_3→*HNO_3 line, which is steeper than that of *NO_3→*HNO_3. This suggests that higher electrocatalytic activity can be

achieved by tuning the oxygen affinities of transition metals for which $*NO_3 \rightarrow *HNO_3$ is the PLS.

Selectivity is in addition a key parameter for determining the efficiency of an electrocatalyst too. Concerning the study of this parameter, it is possible to plot the difference between the U_L for the NO_3^-RR and HER against the U_L of NO_3^-RR, for the different TMs. (Figure 3c)

Metals located in the upper-right region exhibit both high activity and high selectivity, consequently, Cu and Ir emerge as the most promising transition metals; however, despite Ir having higher electrocatalytic activity compared to Cu, it also exhibits lower selectivity, making H_2 the dominant product under NO_3^-RR conditions.

Therefore, it can be concluded that the superior performance of Cu compared to the other TMs can be attributed to its d-band center position, which not only optimizes electron transfer during the RDS but also provides a balanced adsorption strength for NO_3^- and reaction intermediates. This balance enhances NO_3^- reduction while suppressing the HER, improving both efficiency and selectivity toward NH_3 production.

4. Design Strategies to Enhance Copper Electrocatalytic Performance

Copper is a promising TM and a more abundant, cost-effective alternative to noble metals, but understanding the key parameters that influence its performance and developing effective design strategies to improve it is essential to reach the targets set by the "Renewable Energy to Fuels through Utilization of Energy-dense Liquids" (REFUEL) program.[39]

This program, set by the Department of Energy (DOE), outlines specific goals for industrial production, including achieving a Faraday efficiency for NH_3 production exceeding 90%, an NH_3 yield rate of 10^{-6} mol s^{-1} cm^{-2} and a current density of 300 mA cm^{-2}.

Various key parameters for copper electrocatalyst have been identified as crucial factors that affect its activity in the NO_3^-RR, including i) size and morphology, ii) facet engineering, iii) defect engineering, iv) support, v) doping, vi) alloying, vii) heterojunction, viii) Single-atom catalysts (SACs). The modulation of these parameters offers a paramount chance to enhance the activity of the electrocatalysts, and the optimization of more parameters is often exploited to achieve synergistic effects (Figure 4).

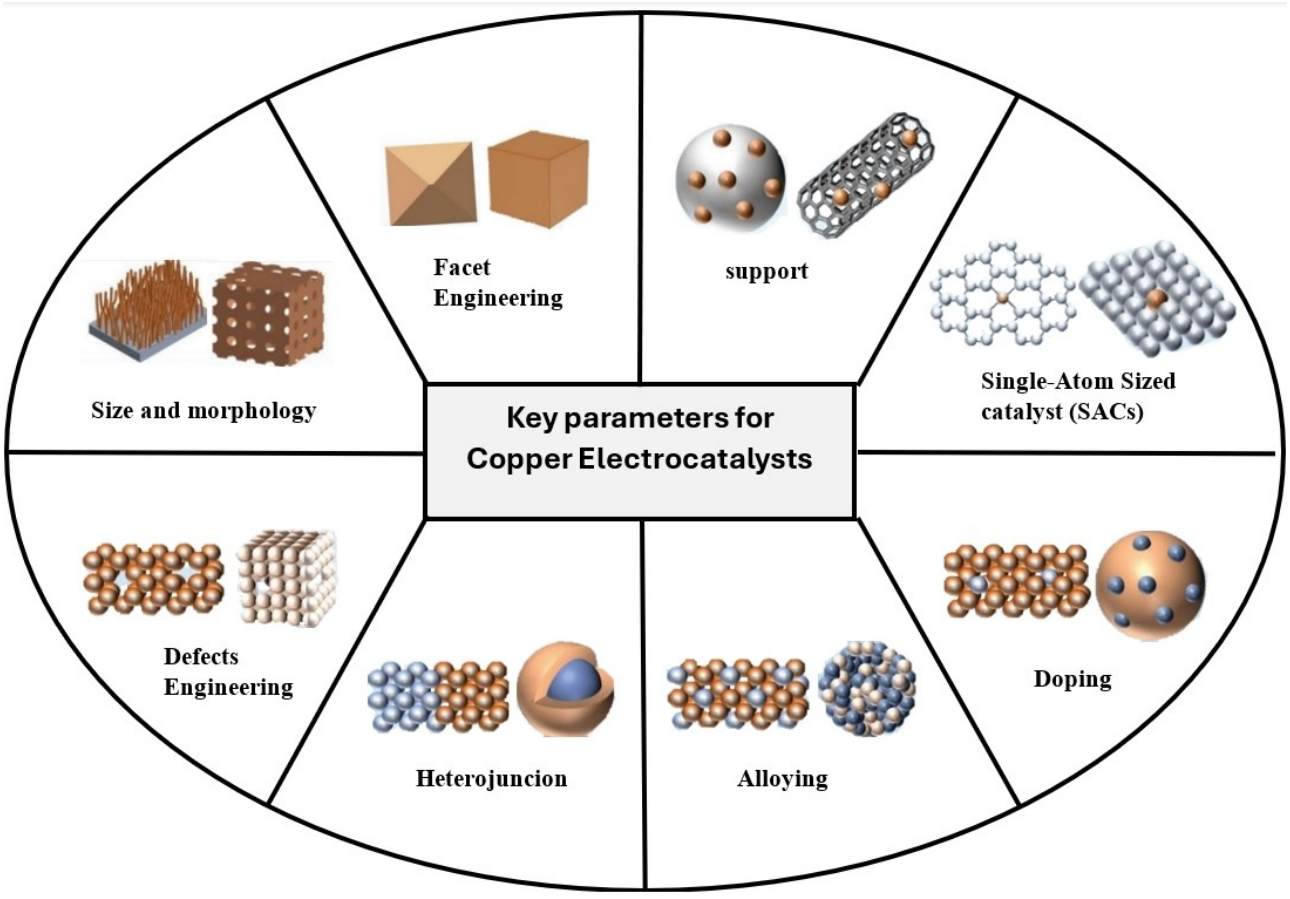

Figure 4. Schematic illustration of key parameters to enhance copper electrocatalytic performance. Adapted from Ref.[40] with permission. Copyright 2024, Wiley, licensed under CC-BY-4.0

In the following sections, a detailed discussion of each of these key parameters is provided, emphasizing their roles in catalysis and exploring various design strategies to enhance the electrocatalytic performance of copper for the NO_3^-RR.

4.1. Size and Morphology

The size and shape of the electrocatalyst particles play a crucial role in determining the electrocatalytic properties of metal electrocatalysts.[41]

Cu foil was among the first materials used as electrocatalysts in the NO_3^-RR, as Dima et al.[32] demonstrated that Cu foil exhibited superior electrocatalytic activity compared to noble metals, such as Au and Ag.

Cu foam has also emerged as a promising electrocatalyst for NO_3^-RR, characterized by its porous structure and extensive surface area, which allow for the exposure of a multitude of active sites. Moreover, its architecture can be easily customized with dopants to further enhance its catalytic performance.[42]

However, this apparent advantage of using highly porous electrocatalyst materials can also become a conceptual disadvantage, particularly when high reaction rates are reached, at which the target reaction becomes limited by the reactant mass transport into the three-dimensional structure of the metal foam electrocatalyst.[43]

In recent years, various processes have been employed to control the morphology of Cu, and several Cu nanostructures have been developed, including Cu nanosheets,[44] Cu nanobelts,[45] Cu nanowires,[34] Cu nanoplates[46] and Cu nanoparticles,[47] which have proven to be superior to both Cu foams and Cu foils.

Fu et al.[44] reported that the FE increased significantly, from 30% for Cu foil to 61% for Cu nanoparticles, accompanied by an approximately 13-fold increase in current density.

Wang et al.[45] developed a 3D Cu nanobelt electrocatalyst that achieves near-complete NO_3^- removal, a significant improvement compared to the 2.6% efficiency of Cu foam. The 3D Cu nanobelt electrocatalyst was prepared by a simple surface oxidation reaction, followed by a chemical reduction process.

Overall, incorporating nanostructures into Cu electrocatalysts offers significant potential for improving NO_3^-RR efficiency by providing a high surface area while mitigating the mass transport limitations typically associated with highly porous materials such as Cu foams.

4.2. Facet Engineering

Gao et al.[48] demonstrated through DFT calculations that the Cu (100) and Cu (111) crystal planes are both thermodynamically favorable. Further insights from Hu et al.[49] confirmed, using RHE calculations, that both Cu (100) and Cu (111) exhibit enhanced electrocatalytic activity compared to Cu (100). Their study also revealed that the competition between NO_3^-RR and HER is influenced by the solution pH, with Cu (100) demonstrating superior electrocatalytic performance for NO_3^-RR in strongly acidic electrolytes, while Cu (111) outperforms in neutral or alkaline conditions. Notably, at pH values below 5.65, HER becomes dominant on Cu (111), reducing its effectiveness for NO_3^-RR and making Cu (100) the more active crystal phase under these conditions.

The difference in electrocatalytic activities is attributed to the local coordination environment and the electronic states of surface atoms on different surfaces. For example, NO_3^- adsorption is favored by a Cu–Cu geometry that closely matches the O–O distance in $*NO_3$, with the Cu–Cu bond length on Cu (111) aligning well with the spacing between the oxygen atoms.

Additionally, the adsorption energy of intermediates is strongly correlated with the position of the d-band center of the electrocatalyst,[50] and the higher d-band center of Cu (111) compared to Cu (100) enhances its adsorption ability for NO_3^-, contributing to its catalytic superiority in suitable pH ranges.

Wu et al.[51] reported the fabrication of uniform Cu nanodisks with enhanced Cu (111) crystal planes, obtained by surface-reconstructed triatomic Cu clusters. These nanodisks achieved a high ammonia yield rate of 2.16 $mg\,mg^{-1}\,h^{-1}$ and a maximum FE of 81.1% at −0.5 V vs RHE.

Similarly, Fu et al.[44] reported that (111) facet-exposed Cu nanosheets, prepared through solution-phase-synthesis, achieve an ammonia formation rate of 0.39 $mg\,mg^{-1}$ Cu h^{-1} and a FE of 99.7% at −0.15 V vs RHE.

In summary, the electrocatalytic performance of Cu is strongly influenced by the exposed crystal planes, with Cu (100) being more effective in acidic environments and Cu (111) excelling under neutral or alkaline conditions. Therefore, exposing specific crystal planes based on operational conditions can significantly enhance the efficiency of NO_3^-RR.

4.3. Defects Engineering

Defect engineering can disturb the periodic structures of lattice to induce the redistribution of the electrocatalyst electronic structure.[52] Importantly, the design and fine modulation of structural defects in Cu-based nanostructures for selective nitrate-to-ammonia reduction is rarely reported.

An example is Xu et al.[46] who synthesized defect-rich Cu nanoplates (dr-Cu NPs), obtained by in situ electroreduction of pre-synthesized CuO nanoplates (CuO NPs) as starting materials. In dr-Cu NPs, the defect-rich structure alters the surface atomic charge distribution compared to an ideal lattice, improving the charge transfer between the electrocatalyst and the electrolyte and promoting the adsorption and conversion of reaction intermediates. Additionally, atomic defects generated from oxygen loss and phase transitions lead to the formation of pits, steps, and irregular edges on the surface, increasing the number of active sites and facilitating the adsorption, enrichment and confinement of reagents and reaction intermediates on the catalyst surface.

Consequently, the electrocatalyst exhibited improved NH_3 production rate and FE compared to Cu nanoplates, achieving

values of 781.25 mg h^{-1} mg^{-1}, and 81,99%, respectively. In conclusion, defect engineering is an effective way to promote catalytic performance by optimizing the interfacial charge transfer and the adsorption of reagents and reaction intermediates on the catalyst surface.

4.4. Support

Morphology control alone may not be sufficient to optimize the electrocatalytic performance, and selecting appropriate electrocatalyst supports to disperse Cu could enable support-metal interactions and improve charge and mass transport kinetics.[53]

Carbon-based materials, such as carbon nanotubes, graphene, carbon black, and conjugated polymers, are widely used as support materials due to their porous structure, varied morphologies, high electrical conductivity, and large specific surface area.[54]

For example, Song et al.[47] encapsulated Cu nanoparticles within a porous carbon framework (Cu@C), achieving an FE of 72.0% at −0.3 V vs RHE, which is 3.6 times higher than that of Cu nanoparticles.

The Cu@C electrocatalyst was synthesized by pyrolyzing the Cu- Benzene-1,3,5-tricarboxylate (BTC) metal-organic framework (MOF) at 700 °C in H_2 atmosphere. The porous carbon framework generates an "enrichment effect," concentrating NO_3^- near the active sites, thereby facilitating mass transfer and enhancing the reaction rate. Additionally, the carbon framework reduces the charge transfer resistance (Rct) of Cu@C compared to Cu, enabling more efficient electron transfer. Overall, employing carbon-based support represents a promising strategy to optimize charge and mass transport.

4.5. Doping

The incorporation of modifier elements is recognized as an effective approach to adjusting the electronic properties of metals.[55]

Among various dopants, boron (B) stands out due to its electron configuration ($2s^2$ $2p^1$), which includes an empty orbital capable of readily accepting electrons from Cu. Zhang et al.[56] produced Cu doped with B (Cu(B)), where the empty orbital of B receives electrons from Cu, modifying its local electronic states. In fact, theoretical and experimental results acknowledge that B-doping increases Cu^+ concentration and upshifts the d-band center of Cu, improving the NO_3^- to NH_3 conversion activity. The Cu(B) electrocatalyst was prepared via a simple low-temperature chemical reduction process, using copper chloride ($CuCl_2$) as precursor and sodium borohydride ($NaBH_4$) as both the B source and reducing agent under the Ar atmosphere. Under 100 ppm NO_3^- electrolyte, this electrocatalyst exhibits a remarkable 100% FE and a high NH_3 yield rate of 0,31 mmol h^{-1} mg^{-1}.

Similarly, Gou et al.[57] also reported efficiently utilizing B-doped Cu nanowires as an electrocatalyst, denoted as B–Cu NWs/CF. The electrocatalyst was synthesized via an oxidation-reduction method. Initially, Cu $(OH)_2$ nanowires were grown in situ on the Cu foam through the oxidation of Cu using a solution of NaOH and $(NH_4)_2S_2O_8$. Subsequently, $NaBH_4$ was used also in this case as both the B source and reducing agent, resulting in the final B–Cu NWs/CF structure. DFT calculations confirmed that the successful incorporation of B into Cu nanowires effectively inhibited HER and the production of other by-products.

Overall, the activity of the electrocatalyst can be further boosted by heteroatom dopants due to local interfacial charge redistribution.

4.6. Alloying

Despite the good electrocatalytic performance of Cu single crystals, their *H adsorption capacity is low, hindering hydrogenation reactions.[58] To improve this aspect, the inclusion of noble metals such as Pd,[59] Pt,[60] Au,[61] Ru,[62][63] and Rh[34] has been implemented.

For example, Liu et al.[34] obtained Cu nanowires coated with Rh clusters and single atoms (Rh@Cu NWs). They were synthesized by first fabricating Cu_2O nanowires, which were electrochemically reduced to Cu nanowires, followed by a galvanic replacement reaction with Rh^{3+} ions to deposit Rh clusters and single atoms on the Cu surface. The synergistic electrocatalytic cooperation between Rh and Cu sites effectively accelerates the surface hydrogenation rate, allowing a very high NH_3 yield rate. Fairly, insufficient doping of Rh may not show a clear synergistic effect between Cu and Rh, while an excessive loading will favor competing HER. Hence, Cu sites preferentially stabilize reaction intermediates, while Rh sites adsorb *H, which are then transferred to the intermediates absorbed on Cu sites, which is confirmed by different investigations, including Electron Paramagnetic Resonance (EPR).

Alloying Cu with another metal to create bimetallic electrocatalysts is another effective strategy, similar to the use of heteroatom dopants, to regulate its electronic structure. For instance, Wang et al.[64] recently synthesized CuNi alloys with various compositions, where Ni allowed the regulation of the affinity of intermediates, favoring their adsorption on the surface of Cu. Studies conducted by Ultraviolet Photoelectron Spectroscopy (UPS) show how increasing the Ni composition in the alloys results in a shift of the d-band center towards the Fermi level, resulting in a decrease in anti-bonding occupancy and stronger bonding of intermediates, which is also confirmed by DFT calculations.

However, the introduction of an excessive amount of Ni, as in the case of $Cu_{30}Ni_{70}$, significantly affects the affinity of intermediates, lowering selectivity and activity.

In summary, alloying Cu with a second metal could introduce synergistic effects that enhance catalytic performance by creating new active phases and regulating electronic structures. This approach optimizes intermediate adsorption and offers a path to overcome the limitations of Cu single crystals, like its low *H adsorption capacity.

4.7. Heterojunction

In electrocatalysis, interactions at the interface between different phases are essential for influencing catalytic performance.[65]

Wang et al.[66] synthesized CuO nanowires (NWAs) by heat treatment of Cu $(OH)_2$ in the presence of oxygen, which were then converted into Cu/Cu_2O NWAs in situ during the electrochemical process.

The conversion process from CuO NWAs to Cu/Cu_2O NWAs was confirmed by in situ Raman spectroscopy, which revealed a gradual disappearance of the characteristic peaks of CuO with increasing applied potential, accompanied by the emergence of the characteristic peaks of Cu_2O. (Figure 5a) Furthermore, the Low-Mass Metal Auger Electron Spectroscopy (LMM AES) spectrum made after the electrochemical reduction, shows the presence of characteristic peaks of both Cu and Cu^+, while the peak of Cu^{2+} is absent; this confirms the conversion process and the presence of Cu, whose signal was not visible in the Raman spectroscopy. (Figure 5b) The Cu/Cu_2O interface was proved as the active site.

Combined results from Differential Electrochemical Mass Spectrometry (DEMS) and DFT calculations demonstrated that the electron transfer from Cu_2O to Cu at the interface facilitates the formation of the *NOH intermediate compared with Cu, suppressing competitive HER, and leading to high activity and high selectivity. (Figure 5 c, d)

Inspired by this work, Xu et al.[67] produced Cu nanowires with surface layers of $Cu_{2+1}O$ (Cu@$Cu_{2+1}O$ NWs). In this structure, the Cu core ensures high electron conductivity, while the $Cu_{2+1}O$ layer offers abundant catalytic sites. Moreover, the electronic interaction at the Cu/$Cu_{2+1}O$ interface shifts the d-band center, effectively modulating the adsorption energies of intermediates.

Overall, constructing heterojunction structures in electrocatalysis has proven to be a highly effective strategy for enhancing catalytic performance. For instance, the interfacial interactions between distinct phases, such as Cu and Cu_2O, play a crucial role in stabilizing reaction intermediates and suppressing competing HER.

4.8. Single-Atom Catalysts (SACs)

Single-atom electrocatalysts (SACs) have recently attracted increasing attention due to their maximum efficiency in utilizing atoms and superior electrocatalytic performance, demonstrating significant potential also as electrocatalysts for the NO_3^-RR.

The main advantages of SACs are provided by:

a. High activity is due to fully exposed active sites and low-coordination metal centers that facilitate the adsorption and conversion of reactive species.[68]
b. High selectivity due to isolated active sites minimizes the possibility for two intermediates located on adjacent sites to form coupled N_2 products, such as N_2O, N_2, or N_2H_4.[69]
c. Appreciable stability is due to strong interactions between the individual atoms and the surrounding coordinating atoms, which stabilize and protect the metal centers.,[70][71]

Considering this family of electrocatalysts, Chen et al.[72] synthesized O–Cu-PTCDA incorporating an optimum content of Cu in an organic molecular solid (3,4,9,10-perylenetetracarbox-

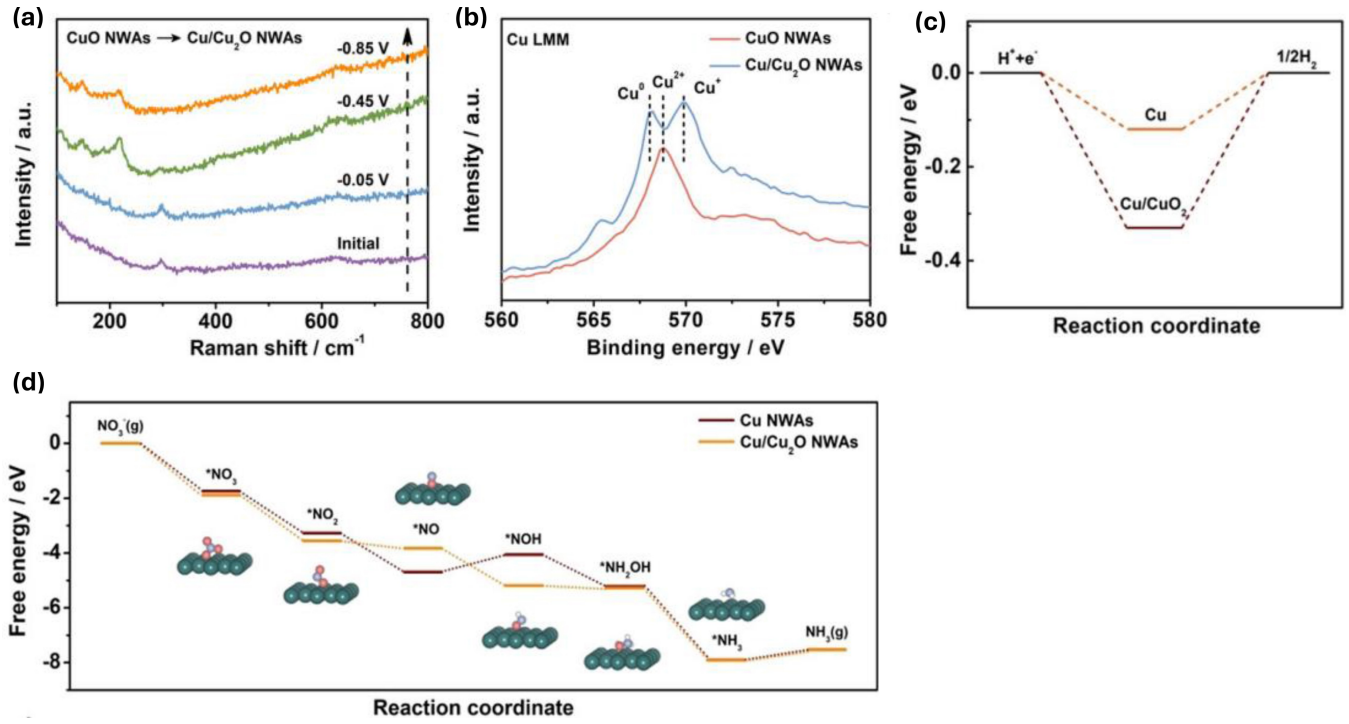

Figure 5. (a) In situ electrochemical Raman spectra of CuO NWAs at different potentials (b) Cu LMM AES spectra (c) The reaction energies of H_2 formation over Cu/Cu_2O NWAs and Cu NWAs. (d) Free-energy diagram of NO_3RR on Cu NWAs and Cu/Cu_2O NWAs. Adapted with permission from Ref.,[66] Copyright 2020, Wiley.

ylic dianhydride, PTCDA), however low NH_3 yield rate is obtained.

Modulating the coordination environment of Cu is thus a crucial strategy for enhancing the performance of atomically dispersed Cu electrocatalysts. In this regard, Gao et al.[71] modified crystalline Th-BPYDC (2,2′-bipyridine-5,5′-dicarboxylic acid, BPYDC) to obtain Cu@Th-BPYDC, where the Cu sites exhibited a novel square unsaturated coordination structure determined by single-crystal X-ray diffraction. Interestingly, it results in a strategy for combining NH_3 production and storage. In fact, authors report that the open single-site Cu serves both as an electro-catalytic active site to promote the NO_3RR and as a Lewis acid center to enhance the interaction with NH_3 molecules.

Another example is shown by Cheng et al,[73] where Cu-cis-N_2O_2 was designed and fabricated. This electrocatalyst presents a symmetry-broken Cu single-atom with Cu coordinated by two N and two O atoms in the cis-configuration, rendering the active site more polar; thus, it's able to accumulate more NO_3^- near the surface and reduce the energy barrier for the formation of the key reaction intermediate *NOH by forming a π-complex.

Several studies have demonstrated that Cu-based diatomic sites exhibit superior electrocatalytic performance compared to Cu-based single-atomic sites.

For instance, Wang et al.[74] reported a Cu/Ni–N–C electrocatalyst, where Ni, allows the regulation of intermediates affinity, favoring their adsorption on the Cu surface.

To sum up, creating a single atom size offers unique advantages, including maximized atomic utilization, high selectivity through isolated active sites, and appreciable stability due to strong coordination with surrounding atoms. These properties, combined with strategies like modulating the coordination environment and integrating diatomic sites, position SACs as promising candidates for advancing NO_3^-RR performance.

4.9. Comparison Among the Different Cu-Based Electrocatalysts

As anticipated in the previous sections, particular attention has been recently dedicated to the development of Cu-based electrocatalysts. For this reason, on the basis of the key parameters that influence the activity and selectivity of copper for NO_3^-RR (i.e. the structural, morphological and surface properties of the electrocatalysts as discussed in sections 4.1–4.8), the recent materials developed in the last three years are reported in Table 1. The aim is to summarize the more recent achievements and to provide a future pathway for the design of future innovative materials, indicating the most influencing parameters to be modulated. For each reported Cu-based electrocatalyst, the NH_3 Faradaic efficiency (FE) and the ammonia yield rate are provided, along with the specific parameters that were modulated to achieve these results. (Table 1)

5. Conclusions

NO_3RR is being recognized as a sustainable approach to synthesizing ammonia which is essential for the chemical industry and a key agricultural input conventionally produced through the hard-to-abate Haber Bosch process. However, there is inherent competition between the NO_3RR and HER and the development of efficient electrocatalysts with specific structures capable of suppressing competitive reactions is crucial.

Among the transition metals, Cu emerged as a promising electrocatalyst thanks to its d-band center position, which not only optimizes electron transfer during the RDS but also provides a balanced adsorption strength for NO_3^- and reaction intermediates. This balance enhances NO_3^- reduction while suppressing the HER, improving both efficiency and selectivity toward NH_3 production. Furthermore, from an economic point of view, its higher availability and low cost compared to most of the noble metals make it particularly suitable for large-scale application.

Then, various key parameters have been identified as crucial factors that affect its activity in the NO_3^-RR and a detailed discussion of each of these has been provided, emphasizing their roles in catalysis and exploring various design strategies

The design of Cu electrocatalysts through nanostructuring has proven effective in providing a high surface area and exposing additional active sites while the introduction of atomic-scale defects optimizes the interfacial charge transfer and the adsorption of reagents and reaction intermediates on the catalyst surface.

Furthermore, facet engineering has shown that specific crystal planes, such as Cu (100) and Cu (111), exhibit unique catalytic properties depending on the pH of the solution. Cu (100) demonstrates superior performance in acidic conditions, while Cu (111) excels under neutral and alkaline conditions, highlighting the importance of tailoring the exposed planes to operational conditions for maximizing efficiency.

The integration of carbon-based support offers additional advantages, such as improved charge and mass transport kinetics while the incorporation of heteroatom dopants introduces local charge redistribution effects that stabilize reaction intermediates and suppress HER, resulting in increased Faradic Efficiencies. Similarly, alloying Cu with other metals to create bimetallic electrocatalysts, is an effective strategy to regulate Cu electronic structure, shifting the d-band center towards the Fermi level, resulting in a decrease in anti-bonding occupancy and stronger bonding of intermediates.

Bimetallic electrocatalysts can also function as tandem systems, where Cu sites preferentially stabilize reaction intermediates, while the second metal adsorbs *H, subsequently transferring it to the intermediates on Cu sites. This approach accelerates the surface hydrogenation rate, effectively addressing the low *H adsorption capacity of Cu. The heterojunction is another effective strategy in electrocatalysis, utilizing interfacial interactions between distinct phases, such as Cu and Cu_2O, to stabilize reaction intermediates and suppress the competing HER.

Table 1. Recently reported Cu-based electrocatalyst for NO_3^-RR. For each material, it is reported: the nature of the electrocatalysts, the experimental conditions (electrolyte), the performances expressed as i) Faradaic Efficiency (FE), ii) ammonia yield rate, iii) current density and iv) potential. In the last column, the key parameters that were modulated are highlighted.

Electrocatalyst	Electrolyte	FE (%)	NH3 yield rate	Current Density (mA cm^{-2})	Potential (vs RHE)	Key Parameters*	Ref.
Cu foil	10 mMKNO_3, 0.1 M KOH	30	3.9 ug h^{-1} cm^{-2}	~ −0.36	−0.15	–	[44]
Cu nanoparticle	10 mMKNO_3, 0.1 M KOH	61	0.22 mg h^{-1} cm^{-2}	~ −4.65	−0.15	1	[44]
(111) facet exposed Cu nanosheets	10 mMKNO_3, 0.1 M KOH	99.7	0.39 mg h^{-1} cm^{-2}	~ −4.92	−0.15	1, 2	[44]
(111) facet exposed Cu nanodisk	10 mMKNO_3, 0.1 M KOH	81.1	2.16 mg mg^{-1} h^{-1}	–	−0.5	1, 2	[51]
dr-Cu NPs	0.5MK_2SO_4, 50 ppm KNO_3	81.99	0.78 mg mg^{-1} h^{-1}	~ −30	−0.646	1, 3	[46]
Cu@C	1 mM NO_3^-	72	~0.32 mg h^{-1} cm^{-2}	~ −4	−0.3	1, 4	[47]
Cu (B)	0.5 M Na_2SO_4, 0.1 M PO_4^{3-}, 100 ppm NO_3^-	100	0.31 mmol h^{-1} mg^{-1}.	~70	−0.6	1, 5	[56]
V_{cu}-Au_1Cu SAAs	0,1 M KOH, 7,14 mM NO_3^-	98.7	0.55 mg h^{-1} cm^{-2}	–	−0.2	2, 3, 6, 8	[61]
$Cu_{50}Ni_{50}$	1 M KOH, 0.1 M KNO_3	99	–	~ −90	−0.1	1, 6	[64]
Rh@Cu NWs	0.1 M Na_2SO_4, 0.1 M KNO_3	93	~0.76 mmol h^{-1} cm^{-2}	~ −162	−0.2	1, 6	[34]
Cu/Cu_2O NWAs	0.5 M Na_2SO_4, 14,3 mM NO_3^-	95.8	0.24 mmol h^{-1} cm^{-2}	–	−0.196	1, 7	[66]
PdCu/Cu_2O	0.5 M Na_2SO_4, 100 mg L^{-1} NO_3^--N	94.32	0.19 mmol h^{-1} cm^{-2}	~ −50	−0.8	1, 6, 7	[75]
O–Cu-PTCDA	500 ppm NO_3-, 0.1 M PBS	85.9	0.025 mmol h^{-1} cm^{-2}	–	−0.4	8	[72]
Cu@ThBPYDC	1 M KOH, 100 mM KNO_3	~80	~0.3 mmol h^{-1} cm^{-2}	~ −80.7	−0.1	4, 8	[71]
Cu-cis-N_2O_2 SAC	1000 ppm N-KNO_3, 0.5 M Na_2SO_4	88.46	27.84 mg h^{-1} cm^2	~ −366	−1.6	3, 8	[73]
Cu/Ni–N–C	100 ppm $NaNO_3$, 0.5 M Na_2SO4	97.28	0.32 mmol h^{-1} cm^{-2}	–	−0.7	6, 8	[74]

* Key parameters: 1. Size and morphology. 2. Facet Engineering. 3. Defects engineering. 4. Support. 5. Doping. 6. Alloying. 7. Heterojunction. 8. Single-atom catalysts (SACs)

Finally, single-atom electrocatalysts represent a promising avenue, offering exceptional activity and selectivity due to their maximized atomic utilization and isolated active sites.

By modulating the coordination environment of single Cu atoms or incorporating diatomic sites, researchers have further improved the efficiency and stability of these systems.

In conclusion, the combination of nanostructuring, facet and defect engineering, support, doping, alloying, heterojunction and creating SACs have been revealed as efficient strategies to enhance the electrocatalytic performance of Cu. However, despite these advancements, challenges remain. Current mechanistic studies on NO_3RR over Cu are limited, with much of the understanding extrapolated from studies on Pt-based electrocatalysts. Thus, further research is needed to elucidate the electrocatalytic mechanism of NO_3^- reduction to NH_3 specifically on Cu.

As shown in Table 1, some electrocatalysts meet the specific targets for industrial production established by the REFUEL program.[39] However, current tests conducted in 'clean' buffer solutions do not accurately reflect the complexity of real wastewater, not considering the influence of ion contamination, organic pollutants, and solid sediments. Therefore, further evaluation of NO_3-RR performance under realistic conditions still needs to be further evaluated.

Acknowledgements

C.S. would like to acknowledge the NextGeneration EU from the Italian Ministry of Environment and Energy Security POR H2 AdP MMES/ENEA with involvement of CNR and RSE, PNRR - Mission 2, Component 2, Investment 3.5 "Ricerca e sviluppo sull'idrogeno" under the ENEA – UNIMIB agreement (Procedure 1.1.3 PNRR POR H_2).

Conflict of Interests

The authors declare no conflict of interest.

Data Availability Statement

The data that support the findings of this study are available from the corresponding author upon reasonable request.

Keywords: nitrate reduction reaction · ammonia production · Copper electrocatalysts · reaction mechanisms · Faradaic efficiency

[1] B. Wang, T. Li, F. Gong, M. H. D. Othman, R. Xiao, *Fuel Process. Technol.* **2022**, *235*, 107380. doi: 10.1016/j.fuproc.2022.107380.
[2] M. Muhyuddin, G. Zuccante, P. Mustarelli, J. Filippi, A. Lavacchi, L. Elbaz, Y.-H. Chen, P. Atanassov, C. Santoro, *Energy Environ. Sci.* **2024**, *17*, 3739–3752. doi: 10.1039/d4ee00561a.
[3] M. Aziz, A. TriWijayanta, A. B. D. Nandiyanto, *Energies* **2020**, *13*, 3062, doi: 10.3390/en13123062.
[4] A. Valera-Medina, F. Amer-Hatem, A. K. Azad, I. C. Dedoussi, M. de Joannon, R. X. Fernandes, P. Glaborg, H. Hashemi, X. He, S. Mashruk, J. McGowan, C. Mounaim-Rouselle, A. Ortiz-Prado, A. Ortiz-Valera, I. Rossetti, B. Shu, M. Yehia, H. Xiao, M. Costa, *Am. Chem. Soc* **2021**, *35*, 6935–8442, doi: 10.1021/acs.energyfuels.0c03685.
[5] H. S. Ahmed, Z. Yahya, W. Ali khan, A. Faraz, *Clean Energy* **2024**, *8*, 60–72, doi: 10.1093/ce/zkae002.
[6] M. Nazemi, S. R. Panikkanvalappil, M. A. El-Sayed, *Nano Energy* **2018**, *49*, 316–323, doi: 10.1016/j.nanoen.2018.04.039.
[7] R. Strait, M. Nagvekar, *Nitrogen + Syngas* **2010**, *303*.
[8] S. L. Foster, S. L. Perez Bakovic, R. D. Duda, S. Maheshwari, R. D. Milton, S. D. Minteer, M. J. Janik, J. N. Renner, L. F. Greenlee, *Nat. Catal.* **2018**, *1*, 490–500, doi: 10.1038/s41929-018-0092-7.
[9] X. Cui, C. Tang, Q. Zhang, *Adv. Energy Mater.* **2018**, *8*, 1614–6832, doi: 10.1002/aenm.201800369.
[10] A. Menció, J. M. Pla, N. Otero, O. Regas, M. B. Roura, R. Puig, J. Bach, C. Domenech, M. Zamorano, D. Brusi, A. Folch, *Sci. Total Environ.* **2016**, *539*, 241–251, doi: 10.1016/j.scitotenv.2015.08.151.
[11] S. Kotopoulou, A. Zampelas, E. Magriplis, *Nutr. Rev.* **2022**, *80*, 762–773, doi: 10.1093/nutrit/nuab113.
[12] G. M. Taylor, R. S. Avera, C. C. Strachan, C. M. Briggs, J. P. Meddler, C. M. Pafford, T. B. Gant, *Oxf. Med. Case Rep.* **2021**, *2021*, 55–58, doi: 10.1093/omcr/omaa136.
[13] Nitrate and Nitrite in Drinking-water Background document for development of WHO Guidelines for Drinking-water Quality, *WHO*, **2004**.
[14] F. Rezvani, M. H. Sarrafzadeh, S. Ebrahimi, H. M. Oh, *Environ. Sci. Pollut. Res. Int.* **2019**, *26*, 1124–1141, doi: 10.1007/s11356-017-9185-0.
[15] Y. Zeng, C. Priest, G. Wang, G. Wu, *Small Methods* **2020**, *4*, 2000672, doi: 10.1002/smtd.202000672.
[16] C. Smith, A. K. Hill, L. Torrente-Murciano, *Energy Environ. Sci.* **2020**, *13*, doi: 10.1039/c9ee02873k.
[17] J. Li, G. Zhan, J. Yang, f. Quan, C. Mao, Y. Liu, B. Wang, F. Lei, L. Li, A. W. M. Chan, L. Xu, Y. Shi, Y. Du, W. Hao, P. K. Wong, J. Wang, S. X. Dou, L. Zhang, J. C. Yu, *J. Am. Chem. Soc.* **2020**, *142*, 7036–7046, doi: 10.1021/jacs.0c00418.
[18] J. Y. Zhu, Q. Xue, Y. Y. Xue, Y. Ding, F. M. Li, P. Jin, P. Chen, Y. Chen, *ACS Appl. Mater. Interfaces* **2020**, *12*, 14064–14070, doi: 10.1021/acsami.0c01937.
[19] J. Lim, C. Y. Liu, J. Park, Y. H. Liu, T. P. Senftle, S. W. Lee, M. C. Hatzell, *ACS Catal.* **2021**, *11*, 7568–7577, doi: 10.1021/acscatal.1c01413.
[20] X. Deng, Y. Yang, L. Wang, X. Z. Fu, J. L. Luo, *Adv. Sci.* **2021**, *8*, 2004523, doi: 10.1002/advs.202004523.
[21] M. S. El-Deab, *Electrochim. Acta* **2004**, *49*, 1639–1645, doi: 10.1016/j.electacta.2003.11.025.
[22] M. Karamad, T. J. Goncalves, S. Jimenez-Villegas, I. D. Gates, S. Siahrostami, *Faraday Discuss.* **2022**, *243*, 502–519, doi: 10.1039/d2fd00145d.
[23] S. Wang, H. Gao, L. Li, K. S. Hui, D. A. Dinh, S. Wu, S. Kumar, F. Chen, Z. Shao, K. N. Hui, *Nano Energy* **2022**, *100*, 107517, doi: 10.1016/j.nanoen.2022.107517.
[24] H. Wan, A. Bagger, J. Rossmeisl, *Angew. Chem. Int. Ed.* **2021**, *60*, 21966–21972, doi: 10.1002/anie.202108575.
[25] I. Katsounaros, G. Kyriacou, *Electrochim. Acta* **2007**, *52*, 6412–6420, doi: 10.1016/j.electacta.2007.04.050.
[26] D. Xu, Y. Li, L. Yin, Y. Ji, J. Niu, Y. Yu, *Front. Environ. Sci. Eng* **2018**, *12*, 523808, doi: 10.1007/s11783-018-1033-z.
[27] J. Gao, B. Jiang, C. Ni, Y. Qi, X. Bi, *Chem. Eng. J.* **2020**, *382*, 123034, doi: 10.1016/j.cej.2019.123034.
[28] H. O. N. Tugaoen, S. Garcia-Segura, K. Hristovski, P. Westerhoff, *Sci. Total Environ.* **2017**, *599*, 1524–1551, doi: 10.1016/j.scitotenv.2017.04.238.
[29] S. V. Lymar, H. A. Schwarz, G. Czapski, *J. Phys. Chem. A* **2002**, *106*, 7245–7250, doi: 10.1021/jp026107l.
[30] T. Hu, C. Wang, M. Wang, C. M. Li, C. Guo, *ACS Catal.* **2021**, *11*, 14417–14427, doi: 10.1021/acscatal.1c03666.
[31] E. Pérez-Gallent, M. C. Figueiredo, I. Katsounaros, M. T. M. Koper, *Electrochim. Acta* **2017**, *227*, 77–84, doi: 10.1016/j.electacta.2016.12.147.
[32] G. E. Dima, A. C. A. De Vooys, M. T. M. Koper, *J. Electroanal. Chem.* **2003**, *554*, 15–23, doi: 10.1016/S0022-0728(02)01443-2.
[33] D. De, E. E. Kalu, P. P. Tarjan, J. D. Englehardt, *Chem. Eng. Technol.* **2004**, *27*, 56–64, doi: 10.1002/ceat.200401832.
[34] H. Liu, X. Lang, C. Zhu, J. Timoshenko, M. Ruschen, L. Bai, N. Guijarro, H. Yin, Y. Peng, J. Li, Z. Liu, W. Wang, B. R. Cuenya, J. Luo, *Angew. Chem. Int. Ed.* **2022**, *61*, 202202556, doi: 10.1002/anie.202202556.
[35] W. Wen, P. Yan, W. Sun, Y. Zhou, X. Y. Yu, *Adv. Funct. Mater.* **2023**, *33*, 2212236, doi: 10.1002/adfm.202212236.
[36] F. Abild-Pedersen, J. Greeley, F. Studt, J. Rossmeisl, T. R. Munter, P. G. Moses, E. Skúlason, T. Bligaard, J. K. Nørskov, *Phys. Rev. Lett.* **2007**, *99*, 016105, doi: 10.1103/PhysRevLett.99.016105.
[37] C. A. Casey-Stevens, H. Ásmundsson, E. Skúlason, A. L. Garden, *Appl. Surf. Sci.* **2021**, *552*, 149063, doi: 10.1016/j.apsusc.2021.149063.
[38] B. Hammer, J. K. Nørskov, *Adv. Catal.* **2000**, *45*, 71–129, doi: 10.1016/S0360-0564(02)45013-4.
[39] G. Soloveichik, M. Acharya, H. Cheeseman, D. Wicks, **2016**.
[40] M. Zheng, J. Zhang, P. Wang, H. Jin, Y. Zheng, S. Z. Qiao, *Adv. Mater.* **2024**, *36*, 2307913, doi: 10.1002/adma.202307913.
[41] L. Liu, A. Corma, *Chem. Rev.* **2018**, *118*, 4887–5264, doi: 10.1021/acs.chemrev.7b00776.
[42] Y. Wang, A. Dutta, A. Iarchuk, C. Sun, S. Vesztergom, P. Broekmann, *ACS Catal.* **2023**, *13*, 8169–8182, doi: 10.1021/acscatal.3c00716.
[43] A. Iarchuk, A. Dutta, P. Broekmann, *J. Hazard. Mater.* **2022**, *439*, doi: 10.1016/j.jhazmat.2022.129504.
[44] X. Fu, X. Zhao, X. Hu, K. He, Y. Yu, T. Li, Q, Tu, X. Qian, Q. Yue, M. R. Wasielewski, Y. Kang, *Appl Mater Today* **2020**, *19*, 100620, doi: 10.1016/j.apmt.2020.100620.
[45] X. Wang, M. Zhu, G. Zeng, X. Liu, C. Fang, C. Li, *Nanoscale* **2020**, *12*, 9385–9391, doi: 10.1039/c9nr10743f.
[46] Y. Xu, M. Wang, K. Ren, T. Ren, M. Liu, Z. Wang, X. Li, L. Wang, H. Wang, *J. Mater. Chem. A* **2021**, *9*, 16411–16417, doi: 10.1039/d1ta04743d.
[47] Z. Song, Y. Liu, Y. Zhong, Q. Guo, J. Zeng, Z. Geng, *Adv. Mater.* **2022**, *34*, 2204306, doi: 10.1002/adma.202204306.
[48] Q. Gao, H. S. Pillai, Y. Huang, S. Liu, Q. Mu, X. Han, Z. Yan, H. Zhou, Q. He, H. Xin, H. Zhu, *Nat. Commun.* **2022**, *13*, 2338, doi: 10.1038/s41467-022-29926-w.
[49] T. Hu, C. Wang, M. Wang, C. M. Li, C. Guo, *ACS Catal.* **2021**, *11*, 14417–14427, doi: 10.1021/acscatal.1c03666.
[50] J. K. Nørskov, F. Abild-Pedersen, F. Studt, T. Bligaard, *Proc. Natl. Acad. Sci. USA* **2011**, *108*, 937–943, doi: 10.1073/pnas.1006652108.
[51] K. Wu, C. Sun, Z. Wang, Q. Song, X. Bai, X. Yu, Q. Li, Z. Wang, H. Zhang, J. Zhang, X, Tong, Y. Liang, A. Khosla, Z. Zhao, *ACS Materials Lett.* **2022**, *4*, 650–656, doi: 10.1021/acsmaterialslett.2c00149.
[52] W. Li, D. Wang, Y. Zhang, L. Tao, T. Wang, Y. Zou, Y. Wang, R. Chen, S. Wang, *Adv. Mater.* **2020**, *32*, 1907879, *Wiley-VCH Verlag*. doi: 10.1002/adma.201907879.
[53] J. S. Elias, K. A. Stoerzinger, W. T. Hong, M. Risch, L. Giordano, A. N. Mansour, Y. Shao-Horn, *ACS Catal.* **2017**, *7*, 6843–6857, doi: 10.1021/acscatal.7b01600.
[54] B. Li, C. Lai, M. Zhang, G. Zeng, S. Liu, D. Huang, L. Qin, X. Liu, H. Yi, F. Xu, N. An, L. Chen, *Adv. Energy Mater.* **2020**, *10*, 2000177, doi: 10.1002/aenm.202000177.
[55] A. Zhang, Y. Liang, H. Zhang, Z. Geng, J. Zeng, *Chem. Soc. Rev.* **2021**, *50*, 9817–9844, doi: 10.1039/d1cs00330e.
[56] L. H. Zhang, Y. Jia, J. Zhan, G. Liu, G. H. Liu, F. Li, F. S. Yu, *Angew. Chem. Int. Ed.* **2023**, *62*, 202303483, doi: 10.1002/anie.202303483.
[57] F. Gou, H. Wang, M. Fu, Y. Jiang, W. Shen, R. He, M. Li, *Appl. Surf. Sci.* **2023**, *612*, 155872, doi: 10.1016/j.apsusc.2022.155872.
[58] J. Wei, Y. Li, H. Lin, X. Lu, C. Zhou, Y. Yun Li, *Environ. Sci. Ecotech* **2024**, *20*, 100383. doi: 10.1016/j.ese.2023.100383.
[59] J. Lim, Y. Chen, D. A. Cullen, S. W. Lee, T. P. Senftle, M. C. Hatzell, *ACS Catal.* **2023**, *13*, 87–98, doi: 10.1021/acscatal.2c04841.

[60] G. Antonio Cerrón-Calle, A. S. Fajardo, C. M. Sánchez-Sánchez, S. Garcia, *Appl. Catal. B* **2022**, *302*, 120844, doi: 10.1016/j.apcatb.2021.120844.
[61] Y. Zhang, X. Chen, W. Wang, L. Yin, J. C. Crittenden, *Appl. Catal. B* **2022**, *310*,121346, doi: 10.1016/j.apcatb.2022.121346.
[62] N. Q. Tran, G. H. Lee, W. M. Liu, K. S. Lim, J. H. Ahn, J. W. Jang, M. H. Lee, *Chem. Commun.* **2022**, *58*, 5257–5260, doi: 10.1039/d2cc00331g.
[63] F. Y. Chen, Z. Y. Wu, S. Gupta, D. J. Rivera, S. V. Lambeets, S. Pecaut, J. Y. T. Kim, P. Zhu, Y. F. Zou, D. M. Meira, G. King, G. Gao, W. Xu, D. A. Cullen, H. Zhou, Y. Han, D. E. Perea, C. L. Muhich, H. Wang, *Nat. Nanotechnol.* **2022**, *17*, 759–767, doi: 10.1038/s41565-022-01121-4.
[64] Y. Wang, A. Xu, Z. Wang, L. Huang, J. Li, F. Li, J. Wicks, M. Luo, D. H. Nam, C. S. Tan, Y. Ding, J. Wu, Y. Lum, C. T. Dinh, D. Sinton, G. Zheng, E. H. Sargent, *J. Am. Chem. Soc.* **2020**, *142*, 5702–5708, doi: 10.1021/jacs.9b13347.
[65] A. Kumar, J. Lee, M. G. Kim, B. Debnath, X. Liu, Y. Hwang, Y. Wang, X. Shao, A. R. Jadhav, Y. Liu, H. Tüysüz, H. Lee, *ACS Nano* **2022**, *16*, 15297–15309, doi: 10.1021/acsnano.2c06747.
[66] Y. Wang, W. Zhou, R. Jia, Y. Yu, B. Zhang, *Angew. Chem.* **2020**, *132*, 5388–5392, doi: 10.1002/ange.201915992.
[67] T. Ren, K. Ren, M. Wang, M. Liu, Z. Wang, H. Wang, X. Li, L. Wang, Y. Xu, *Chem. Eng. J.* **2021**, *426*, 130759, doi: 10.1016/j.cej.2021.130759.
[68] T. Zhang, D. Zhang, X. Han, T. Dong, X. Guo, C. Song, R. Si, W. Liu, Y. Liu, Z. Zhao, *J. Am. Chem. Soc.* **2018**, *140*, 16936–16940, doi: 10.1021/jacs.8b10703.
[69] E. Murphy, Y. Liu, I. Matanovic, S. Guo, P. Tieu, Y. Huang, A. Ly, S. Das, I. Zenyuk, X. Pan, E. Spoerke, P. Atanassov, *ACS Catal.* **2022**, *12*, 6651–6662, doi: 10.1021/acscatal.2c01367.
[70] X. Li, H. Rong, J. Zhang, D. Wang, Y. Li, *Nano Res.* **2020**, *13*, 1842–1855, doi: 10.1007/s12274-020-2755-3.
[71] Z. Gao, Y. Lai, Y. Tao, L. Xiao, L. Zhang, F. Luo, *ACS Cent. Sci.* **2021**, *7*, 1066–1072, doi: 10.1021/acscentsci.1c00370.
[72] G. F. Chen, Y. Yuan, H. Jiang, S. Y. Ren, L. X. Ding, L. Ma, T. Wu, J. Lu, H. Wang, *Nat. Energy* **2020**, *5*, 605–613, doi: 10.1038/s41560-020-0654-1.
[73] X. F. Cheng, J. H. He, H. Q. Ji, H. Y. Zhang, Q. Cao, W. J. Sun, C. L. Yan, J. M. Lu, *Adv. Mater.* **2022**, *34*, 2205767, doi: 10.1002/adma.202205767.
[74] Y. Wang, H. Yin, F. Dong, X. Zhao, Y. Qu, L. Wang, Y. Peng, D. Wang, W. Fang, J. Li, *Small* **2023**, *19*, 2207695, doi: 10.1002/smll.202207695.
[75] H. Yin, Z. Chen, S. Xiong, H. Yamashita, Y. Peng, J. Li, *Chem Catal.* **2021**, *1*, 1088–1103, doi: 10.1016/j.checat.2021.08.014.

Manuscript received: August 2, 2024
Revised manuscript received: December 21, 2024
Version of record online: ■■, ■■

REVIEW

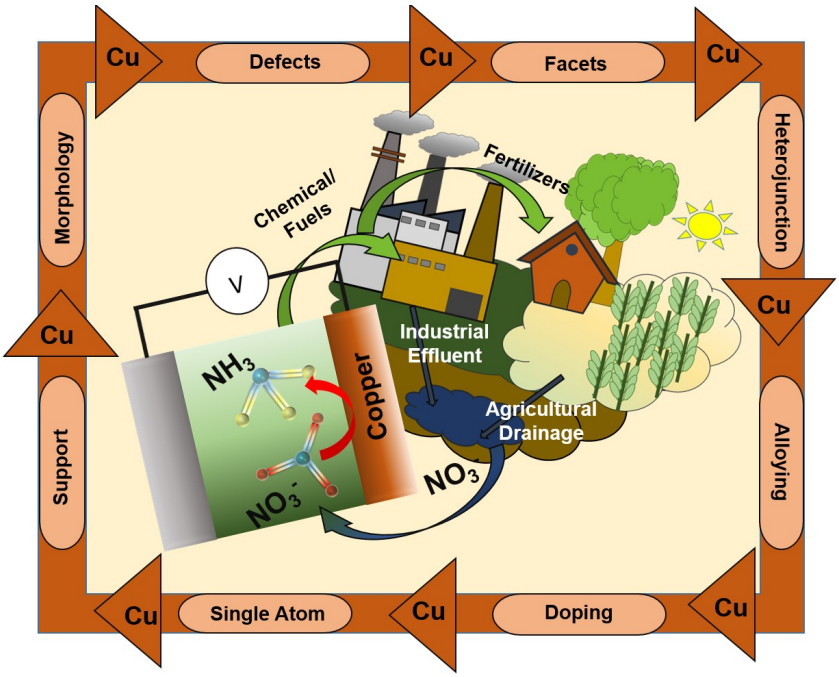

S. Lombardi, S. Mostoni, L. Mirizzi, R. Scotti, R. Viscardi, M. Muhyuddin, Prof. M. D'Arienzo, Prof. C. Santoro**

1 – 15

Design Strategies to Enhance Copper Electrocatalytic Performance for Nitrate-to-Ammonia Electroreduction

Electrochemical nitrate reduction (NO_3^-RR) is an alternative way to synthesizing ammonia. This review focuses on copper-based electrocatalysts and current state of research employing copper-based materials is presented. NO_3^-RR reaction mechanisms are described. Then, various electrocatalyst fabrication routes and designing strategies are reviewed, emphasizing the role of the evolved structure, morphology, textural properties and surface chemistries in improving the reaction kinetics.